Introducing the Ripplet Conversion in Order to Extract the Feature from Iris Images

Daruosh Kavosi[1], Abas Karimi[2]

1. Eslam Abad-E-Gharb Branch,Islamic azad University,Eslam Abad-E-Gharb,kermanshah,Iran.
2. Deaprtment of Computer Engineering,faculty of Engineering,Arak Branch,Islamic azad University,Arak,Markazi,Iran

***Corresponding Author email**:* kavosy.daruosh@gmail.com

Abstract: The growing need for identification systems has led to the design and production of various systems around the world. Hence, providing accurate and powerful methods in this area has become a crucial research challenge. Meanwhile, the use of biometric features to authenticate them has become an interesting idea. One of these biometric properties is the biometric iris. The purpose of this paper is to introduce the transformation of ripplet as a new approach to iris biometrics in order to authenticate individuals. The present research is of a theoretical type and in terms of library and descriptive and analytical method. The research revealed that the ripplet method worked polarly and was able to detect the slightest changes, thus increasing the accuracy of the detection and reducing the error rate. In the proposed method, in order to extract the characteristic of iris images, the ripplet transformation method was used which is one of the main methods in the domain of transformation. In this method, the edge detector and Huff transformations were used to improve the speed and accuracy of the segmentation process. In the feature extraction step, in order to accurately identify individuals, most of the discriminatory information contained in the iris pattern should be extracted. Extracting the attribute at this stage is done using the ripplet transform in the transform domain. In the process of producing code, the iris code is extracted using ripplet transformation.
Keywords: Ripplet conversion, iris images, biometrics, feature extraction, iris code

INTRODUCTION

Authentication research was carried out by the eye iris in 1987, followed by authentication by skeletal, retina, and eye area in 2009. At the moment, several detection and approval systems have been developed, each of which uses one or more biometric ocular features. The idea of using iris as an optical fingerprint was first introduced by Flam and Ambassador. Since then, iris has evolved as a reliable biometric and widely studied. The biometric popularity of the iris has led to widespread use of iris-based authentication systems around the world. Displaying high-quality images or signals is critical for image processing, car vision, and pattern recognition and image compression. Harmonic analysis [1] provides a method for displaying high-quality signals. In particular, harmonic analysis is considered to represent the quality and effectiveness of the signal by the weighting of the base functions. Here we mean the weights, coefficients, and the mapping from the input signal to the coefficients is called transform. In image processing, Fourier transform is usually used. However, Fourier's transform can only be able to provide a high-quality display for smooth and smooth images, and is not effective for images that have an edge. The edges or boundaries of the objects cause discontinuities or singularities in the image intensity. How to display a unique quality in pictures is a big challenge in harmonic analysis. It is well known that the one-dimensional singularities in a function (which have a period of finite or alternating time), disperse the display in the Fourier series of the function, which is referred to as the phenomenon Gibbs. Conversely, the wavelet transform, capable of displaying the quality of a function with one-dimensional singularities [2, 3]. However, the transform of a typical wavelet is not capable of solving the optional two-dimensional singularities, hence the transform of the next-wave vector, the only tensor of the two-dimensional wavelet transforms, which solve the one-dimensional horizontal and vertical singularities, respectively. To overcome the wavelet constraints, transform ridgelet [4.5] is introduced. The transformridgelet can solve one-dimensional singularities in the desired direction (including portrait and landscape orientation). The transformridgelet provides information about the linear edges in the images, hence, this transform is based on transform Radon [6], which is able to extract for arbitrary lines. Therefore, the transformridgelet is not able to solve the two-dimensional singularities, Candes and Donoho, and the first-generation transform curvelet based on multi-scale ridgelet [7, 8] then they proposed a two-generation curvelet [9,10]. The transform curvelet can solve two-dimensional singularities in smooth and smooth curves. The transform curvelet uses a scaling rule to achieve an anisotropic direction. From the perspective of microlocal analysis, the coherent characteristic of the transform curvelet ensures the solving of two-dimensional singularities in C^2 curves [9-12]. Similar to the curvelet, the contourlet [13, 14] and the bandlet [15], proposed two-dimensional singularities. However, it is not

clear why the parabolic scaling for the curvelet is chosen to achieve a disharmonious orientation. Regarding this, two questions arise: is the law of scaleing its contribution to all types of borders optimal? If not, what scale will be optimal? To answer these two questions, the scaling law is generalized, which leads to a new rule called transform Ripplet transform Type-I. The transform Ripplet transform Type-I transforms the curvelet by adding two parameters, namely support c and d. Hence, the transform curvelet is just a special case of transform Ripplet transform Type-I with c = 1 and d = 2. The new parameters, namely support for c and degrees d transform ripplet, provide anomalous representation of singularities in curves that are arbitrarily formed. Considering the importance of the subject, this paper uses the transform ripplet as a new approach to the iris biometrics to authenticate individuals. This method works polarly and can detect the slightest changes, thus increasing the accuracy of detection and reducing the error rate.

The transform ripplet capabilities

The transform ripplet has the following capabilities:

Multi-resolution; transform ripplet provides a hierarchical representation of images. It can consistently approximate thick images with elegant resolution.

Good localization; ripplet functions have intensive compression support in the area of frequency and very fast deterioration in the area. Therefore, the ripplet functions are well focused in both the spatial and frequency domains.

High directionality; ripplet functions in different directional directions. By increasing the resolution, ripplet functions can get more directions.

General scaling and support; ripplet functions can display arbitrary scale and backing.

Anisotropy; general scaling and support Anisotropy results in ripplet functions that are guaranteed to get singularities in different curves.

Fast coefficient decay; the coefficient of transform ripplet decreases faster than other transform coefficients, which means that it has the ability to concentrate more energy.

Continuous transform curvelet

Similar to the definition of wavelets, the entire curvelet family is based on the original curvee functions. The original curve functions vary from course to fine (thick to delicate) scales. Curvelet functions are transitions and rotations of the main functions. The two-dimensional curvelet function is defined below [7,8];

$$\gamma_{a\vec{b}\theta}(\vec{x}) = \gamma_{a\vec{0}o}\left(R_\theta(\vec{x} - \vec{b})\right) \quad (1)$$

Where $R_\theta = \begin{bmatrix} cos\theta & sin\theta \\ -sin\theta & cos\theta \end{bmatrix}$ is a rotary matrix and radians θ rotate around their axis. $\vec{x}$ and $\vec{b}$ are two-dimensional ones. $\gamma_{a\vec{0}o}$ is the main curvelet function. The original curvelet function $\gamma_{a\vec{0}o}$ is defined by the parameter scale a in the frequency domain in polar coordinates [8].

$$\hat{\gamma}_a(r,\omega) = a^{3/4} W(a,r) V(\omega/\sqrt{a}) \quad (2)$$

Which is $\hat{\gamma}_a(r,\omega)$ the Fourier transform $\gamma_{a\vec{0}o}$ in the polar coordinate system. $W(r)$ is the "radial window" and $V(\omega)$ is the "angular window". The two windows have compression (integral) support on [1 / 2,2] and [-1,1], respectively. They meet the following acceptability criteria:

$$\int_{1/2}^{2} W^2(r) \frac{dr}{r} = 1 \quad (3)$$

$$\int_{-1}^{1} V^2(t) dt = 1 \quad (4)$$

The two windows divide the polar frequency domain into the "wedge" shown in Fig. From Equation 2 to 4, we find that the Fourier transform of the curvelet has compressive support in the small region, which is the product of the Cartesian r $r \in [\frac{1}{2a}, \frac{2}{a}]$ and $\omega \in [-\sqrt{a}, \sqrt{a}]$. Also, the curvelet has small effective areas that quickly collapses in the area. In contrast to the wavelets, in addition to the scaling information and position information, the curvelets have a different parameter for displaying directional information. An intuitive way to get directionality information is to use a rotating wavelet. However, the rotating transform curvelet isotropic (convergence) feature creates an inappropriate rotation for solving the wavefront set [9,10]. The parabolic scale used in the definition of curvelets ensures effective area length and width for satisfaction, $width \approx length^2$ and leads to the anisotropic curvelets behavior, so that the transform curvelet is suitable for solving the arbitrary wavefront Creates. Partial scaling is the most important transform curvelet property, as well as the key difference between curvelet and rotational wavelet. According to the two-dimensional integral function $f(\vec{x})$, the continuous transform curve is defined by the internal multiplication $f(\vec{x})$ and the curvelet function [9,10,16].

$$C(a,\vec{b},\theta) = \langle f, \gamma_{a\vec{b}\theta} \rangle = \int f(\vec{x})\overline{\gamma_{a\vec{b}\theta}(\vec{x})}d\vec{x} \quad (5)$$

That $C(a,\vec{b},\theta)$ coefficients curvelet and (.) Represents the conjugate operator. Coefficients curvelet describes the signal's characteristics in different scales, directions, and situations. In fact, the transform curvelet takes only the features of the high frequency component $f(\vec{x})$, so the parameter of the scale a cannot contain an infinite amount. Therefore, a continuous continuous transformation curvelet consists of a transform-curvelet fine-scale and a transform of the coarse-scale isotropic wavelet. Full curvelet transformation is inversely proportional. We can complete the entire reconstruction of the input function based on its wavelet coefficients. With the complete transformation of the curvelet, the parseval formula [9,10,16] is maintained. If $f(\vec{x})$ is a hyperfunction, it can be reconstructed from the coefficients obtained from equation (5)

$$f(\vec{x}) = \int \frac{C(a,\vec{b},\theta)\gamma_{a\vec{b}\theta}(\vec{x})dad\vec{b}d\theta}{a^3} \quad (6)$$

and

$$||f||^2 = \int \frac{|C(a,\vec{b},\theta)|^2 dad\vec{b}d\theta}{a^3} \quad (7)$$

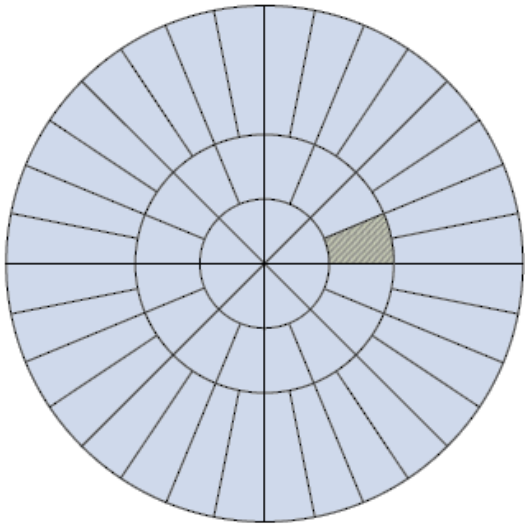

Figure 1. Tiling the polar frequency domain (shaded "wedge" refers to the transform of the original function's frequency)

Continuous ripplet transform

In this section, the ripplet and transform ripplet functions are introduced continuously. First, the curvelet functions are generalized to define ripplet functions, and then a definition of continuous transformation ripplet is provided.

Ripplets

The parabolic scale used in curves leads to solving two-dimensional singularities. However, there is no evidence to show that parabolic scaling is an optimal scaling law. We can define the law of scaling in a broader and more flexible way. The ripplet function can generate the same strategy of equation 1.

$$\rho_{a\vec{b}\theta}(\vec{x}) = \rho_{a\vec{o}o}\left(R_\theta(\vec{x}-\vec{b})\right) \quad (8)$$

Where $\rho_{a\vec{b}\theta}(\vec{x})$ is the main ripplet function and $R_\theta = \begin{bmatrix} cos\theta & sin\theta \\ -sin\theta & cos\theta \end{bmatrix}$ is a rotary matrix. We define the main function of the ripplet in the frequency domain;

$$\hat{\rho}_a(r,\omega) = \frac{1}{\sqrt{c}} a^{\frac{1+d}{2d}} W(a,r) V\left(\frac{a^{\frac{1}{d}}}{c.a}.\omega\right) \quad (9)$$

Which is the $\hat{\rho}_a(r,\omega)$ transform of the Fourier form of $\rho_{a\vec{o}o}(\vec{x})$. $W(r)$ is the radial window on [1/2,2] and $V(\omega)$ is the angle of the window on [-1,1] . They also accept the acceptability conditions (3) and (4). The set of functions $\{\rho_{a\vec{b}\theta}\}$ is defined as ripplet functions, since in the domain of these functions, they have shapes similar to ripplet. C Supports ripplets, and d is defined as ripplet attributes. The curvelet is just a special case of ripplet for c = 1 and d = 2. Figure 2 shows the ripplet with different c and d in the domain. From Fig. 2 it can be seen

that ripplet functions deteriorate rapidly from the effective region, which is an ellipse pointing the main axis in the ripple direction. The main axis is defined as an effective length, and the smaller axis, which is orthogonal to the main axis, is effective. The values of c and d actually affect the effective length and width of ripplets in the area of the place. The effective area has properties for its length and width as follows: $width \approx c \times length^d$. For constant d, c is larger, shorter and longer. When c is constant and d becomes larger, the width becomes shorter and the length becomes longer. An adaptive effective area set by c and degree support d represents the most distinctive feature of ripplet on a global scale. For c = 1 and d = 1, both directions for the axes are ranked in the same way. Therefore, ripplet with d = 1 has no anisotropic behavior. For d> 1, an anisotropy property is assigned to transform ripplet. For d = 2, the ripplets have parabolic scaling. For d = 3, ripplets have cubic scaling. Therefore, Anisotropy ripplet provides the ability to capture singularities in arbitrary curves. Ripplets as the curvelet generalization have almost all curvelet features except parabolic scaling. Ripplets can obtain data multi-resolution analysis. For each scale, ripplets have different compression support, so that ripplettes can focus more closely on the singularities.

Continuous ripplet transform

For a two-dimensional integral function $f(\vec{x})$, the continuous transformation ripplet is defined as the multiplication of the internal $f(\vec{x})$ and ripplet;

$$R(a,\vec{b},\theta) = \langle f, \rho_{a\vec{b}\theta} \rangle = \int f(\vec{x})\overline{\rho_{a\vec{b}\theta}(\vec{x})}d\vec{x} \qquad (3\text{-}10)$$

Where $R(a,\vec{b},\theta)$ is a coefficient of ripplet. When the ripplet function is divided by the curves in the images, the corresponding coefficients will have a large size and the coefficients decay rapidly in the singular direction $a \to 0$. The transform ripplet defined in Equation 10 has the same subject as the transform curvelet, so that continuous transform ripplet can only yield the behavior $f(\vec{x})$ in high frequency bands. To create a continuous ripplet, we need to transform the isotropic wavelet to display low frequency information. However, what is important is the behavior of the transform in high frequency bands, which is the difference between the state of the ripplet and the curvelet. We now transform images into another area called the ripplet domain. The challenge comes when trying to reconstruct images from ripple coefficients. The following theorems introduce an inverse ripplet transform.

Theorem 1. Let f $f \in L^2$ be a hyperfunction, which means that Fourier transform disappears for $|\omega| < 2/a_0$ and a_0 is constant. f can be re generated using its transform ripplet [17];

$$f(\vec{x}) = \int \frac{R(a,\vec{b},\theta)\rho_{a\vec{b}\theta}(\vec{x})dad\vec{b}d\theta}{a^3} \qquad (11)$$

And a maintains the parseval formula for f;

$$||f||_{L_2}^2 = \int \frac{|R(a,\vec{b},\theta)^2 dad\vec{b}d\theta}{a^3} \qquad (12)$$

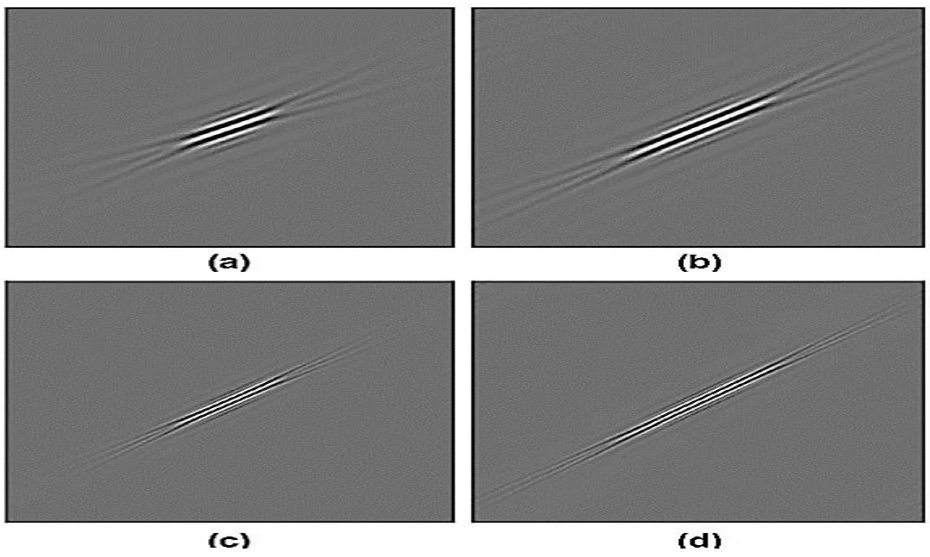

Figure 2 . Ripplets with different c and d in the spatial area

Figure 2 - Ripplets in the area of the location with support and varying degrees of focus, b = 0. (A) a = 3, $\theta = 3\pi/16$, c = 1, d = 2, is called a special curvelet.)b ($a = 3$ ،$\theta = 3\pi/16$ ،$c = 1.5$ ،$d = 2$) .c ($a = 4$ ، $\theta = 3\pi/16$ ،$c = 1$ ،$d = 4$) ،d ($a = 4$ ،$\theta = 3\pi/16$ ،$c = 1.5$ ،$d = 4$.

Theorem 2. Let $f \in L^2$ be. A pure radial function of a finite band Φ exists in L^2 and decreases rapidly, such that if $\Phi_{a_0,b}(x) = \Phi(x - b)$;

$$f(x) = \int \langle \Phi_{a_0,b}, f \rangle \, \Phi_{a_0,b} db + \int_0^{a_0} \int \int \langle f, \rho_{a\vec{b}\theta} \rangle \, \rho_{a\vec{b}\theta}(x) \, da d\vec{b} d\theta / a^3 \quad (13)$$

And

$$||f||^2 = \int |\langle \Phi_{a_0,b}, f \rangle|^2 db + \int_0^{a_0} \int \int |\langle f, \rho_{a\vec{b}\theta} \rangle|^2 da d\vec{b} d\theta / a^3 \quad (14)$$

Since the topic of interest is only good-scale components or high-frequency bands, selecting a transform wavelet for a large scale can be very intolerable. Theorem 2 can be proved with the same argument used in [10] [17].

Discrete transformation ripplet

Digital image processing requires discrete transformations instead of continuous transformations. In this section, the transformation ripplet and its analysis are suggested. In fact, the transform ripplet discontinuity is continuous based on the discretization of the ripplet parameters, which is similar to that of a discrete transform curvelet [16]. For the parameter scale a, we take a sample at dual intervals. The position parameter b and the rotational parameter θ can be sampled at intervals of equal magnitude. a, $\vec{b}$, and θ are replaced by the discrete parameters a_j, $\vec{b}_k$ and θ_l, where $a_j = 2^{-j}$, $\vec{b}_k = [c.2^{-j}.k_1, 2^{-j/d}.k_2]^T$ and $\theta_l = \frac{2\pi}{c}.2^{-\lfloor j(1-1/d) \rfloor}.l$ satisfies, so that $\vec{k} = [k_1, k_2]^T$ ،$(.)^T$ represents the vector vector and j, $\vec{k} = [k_1, k_2]^T$. The degrees of ripplets can yield some of the $\mathbb{R}$. Since each real number can be approximated by rotational numbers, we can show d with $d = n/m$ ،$n, m \neq 0 \in \mathbb{Z}$. Usually, we prefer $n, m \in N$ are both main. In the frequency domain of the corresponding frequency response, the ripplet function is as follows:

$$\hat{\rho}_j(r, \omega) = \frac{1}{\sqrt{c}} a^{\frac{m+n}{2n}} W(2^{-j}.r) V\left(\frac{1}{c}.2^{-\left\lfloor j\frac{m-n}{n} \right\rfloor}.\omega - l\right) \quad (15)$$

That W and V satisfy the acceptable conditions below;

$$\sum_{j=0}^{+\infty} |W(2^{-j}.r)|^2 = 1 \quad (16)$$

$$\sum_{l=-\infty}^{-\infty} |V\left(\frac{1}{c}.2^{-\lfloor j(1-1/d) \rfloor}.\omega - l\right)|^2 = 1 \quad (17)$$

C, d and j are known.

The "wedge" associated with the ripplet function in the frequency domain is as follows:

$$H_{j,l}(r, \theta) = \left\{2^j \leq |r| \leq 2^{2j}, \left|\theta - \frac{\pi}{c}.2^{-\lfloor j(1-1/d) \rfloor}.l\right| \leq \frac{\pi}{2} 2^{-j}\right\} \quad (18)$$

In a discrete state, you can have a better understanding of the parameters c and d. The parameter c controls the number of directions in the high bandwidth. d controls how the number of rows changes across bands. For constant c, d helps control the resolution in directions in any high band. d and c, controls the number of directions in all high bandwidths. c and d determine the total number of directions in each band with each other. The transform ripplet is a discrete image of $M \times N$ ،$f(n_1, n_2)$ as follows:

$$R_{j,\vec{k},l} = \sum_{n_1=0}^{M-1} \sum_{n_2=0}^{N-1} f(n_1, n_2) \overline{\rho_{j,\vec{k},l}(n_1, n_2)} \quad (19)$$

Where $R_{j,\vec{k},l}$ is a coefficient of ripplet. The image can be retrieved via reverse discrete ripplet;

$$f(n_1, n_2) = \sum_j \sum_{\vec{k}} \sum_l R_{j,\vec{k},l} \rho_{j,\vec{k},l}(n_1, n_2) \quad (20)$$

Tight Frame

From the frame's point of view, ripplets provide a new Tight frame with a scattered view for images with discontinuities along C ^ d curves. In order to prove this in the Tight frame, two introductory introductions of the subject are presented to facilitate the proof of the Tight frame. Here are two introductions of the topic required for proof [17]. Introduction Subject 1. We assume that $\{\Phi\} \subset L^2(R^2)$ is a finite band function with the assumption$(\hat{\Phi}) \subset [-\pi A, \pi A] \times [-\pi A, \pi B]$. We assume that $g \in L^2(R^2)$ is defined in the domain of frequency with $\hat{g}(\omega) = |\hat{\Phi}(\omega)|^2 \hat{f}(\omega)$, where $\hat{g}(\omega)$ ،$\hat{\Phi}(\omega)$ ، $\hat{f}(\omega)$ are the transforms of the formations g, Φ and f respectively. If we have the set of functions$\{\Phi_k(x) = \Phi(x_1 - k_1/A, x_2 - k_2/B)\}$, then we have;

$$g(x) = \sum_k \langle f, \Phi_k \rangle \Phi_k(k)$$

And

$$||g||^2 = \sum_k |\langle f, \Phi_k \rangle|^2$$

Introduction Subject 2. The ripplet functions provide a Tight frame with each defined L ^ 2 of the f function.

$$||f||_{L_2}^2 = \sum_{j,\vec{k},l} |R(j, \vec{k}, l)|^2 \quad (3\text{-}21)$$

This proposition can be proved with the transition parameter $\vec{b}$ and $l = 0$ based on the above introduction. For arbitrary l, you can use coordinates to get $\vec{l} = 0$ periods, which is the introduction to subject 1.

Analysis of the feature extraction from iris images using the transform ripplet method

First step: to segment the received image. Since the image is not just an iris image of the eye and includes other parts of the eye such as eyelids, eyelashes, etc., it is necessary to first separate the real iris space in the digital eye view. At this stage, the Edge Detector is used to find the edge of the image of the eye as well as the transformation of the huff to identify the internal and external boundaries of the iris. The edge detector is a multi-stage edge detection technique. Edge detection is one of the methods of image processing that is used to modify Sudden use is made of bright pixel values. In this step of simulation, in order to smooth the image of the Gaussian filter, its mathematical relation is given below;

$$g(m.n) = G(m,n) * f(m,n) \quad (21)$$

In the above relation, G is equal to;

$$G = \frac{1}{2\sigma^2} exp\left(\frac{-(m^2+n^2)}{2\sigma^2}\right) \quad (22)$$

In the following, in order to obtain M (n, n), it is necessary to calculate the gradient g (m.n), so we will result;

$$M(n,n) = \sqrt{(g_m^2(m,n) + g_n^2(m,n)} \quad (23)$$

And

$$(m,n) = tan^{-1}[g_n(m,n)/g_m(m,n)] \quad (24)$$

The threshold M is obtained according to the following equation;

$$M_T(m,n) = \begin{cases} M(m,n) & if \ \ M(m,n) > T \\ 0 & otherwise \end{cases} \quad (25)$$

In the above relation, T is chosen to preserve only all the edges, but a large part of the noise is also suppressed. In the following, in order to narrow the edge of the edge, the pixels that are not multiplied on the

edges obtained from M_T in relation (4-5) are stopped. Thus, if any $M_T(m,n)$ is non-zero, $\theta(m,n)$ then $M_T(m,n)$ remains unchanged, otherwise it is zero. This will result in a previous threshold with two different thresholds T_1 and T_2 for obtaining binary images T_1 and T_2. After this step, the discrete sections of the T_2 edge are joined together to form continuous edges. The next step is to diagnose the iris and pupil border. For this purpose, a circular huff is used to reduce the radius and coordinates of the iris and pupil spaces. The edge of the image is calculated by calculating the first derivative of the intensity values in the eye image and then the results are determined by applying the threshold. By mapping the edge, the huff space is determined for circular cross-sectional parameters through each point. The maximum point in the huff space corresponds to the radius and central coordinates of the best circle defined by the edge points.

Second step: the normalization process. To this point, the iris range was removed from the entire eye area in the image. The iris image may diverge from its normal position for a variety of reasons, including pupil enlargement, variable imaging distance, camera rotation, vertebra, eye rotation in the cavity of the eye, and so on. Because of the image segmentation and the iris in the image, the image needs to be normalized to be used for subsequent processing. The normalization process produces an irisic space that has the same dimensional stability, so that two identical iris shots in different conditions, with the same spatial attributes, are identical. Another thing to note is that pupil space is not always centered in the iris area and is usually slightly prone to nose. The normalization process involves opening the iris and transforming it into its polar equivalent. Mapping the iris space from the Cartesian coordinates to normalize the non-centered polar representation is modeled according to the equation below:

$$I(x(r,\theta),y(r,\theta) \rightarrow I(r,\theta) \quad (26)$$

where in;

$$x(r,\theta) = (I-r)x_p(\theta) + rx_i(\theta)$$
$$y(r,\theta) = (I-r)y_p(\theta) + ry_i(\theta) \quad (27)$$

$I(x,y)$is the iris space image, (x, y) is the original Cartesian coordinate, (r, θ) is the corresponding normalized polar coordinate, and $x_p,y_p$and x_i,y_i are the coordinates of the pupil and iris boundaries along the direction of θ. In this model, the number of data points is selected along each radial line. The pupil center is considered as the reference point, and radial vectors pass through the iris. The number of radial lines around the iris is defined by angular resolution. The normalized pattern, Cartesian coordinates detects the data points from the radius and position of the angle in the normalized pattern.

Third step: Feature extraction is accomplished by complexizing the normalized iris pattern with one-dimensional Gabor logarithmic wavelets. A two-dimensional normalized pattern is broken up in a number of one-dimensional signals, and then these one-dimensional signals are calculated by logarithmic Gabor wavelets using FFT and inverse FFT. Feature extraction at this stage is done using the transform ripplet in the transform domain.

Fourth step: the iris code generation process. Feature is extracted using transform ripplet. Here, a method called quantification of phase is used to generate iris code. In quantum phase, if both real and imaginary parts are + ve, "11" is assigned. If both are real and imaginary -ve then "00", if the real part + ve and the imaginary part-ve, is "10", and if the real part is -ve and the imaginary section + ve, "01" is assigned. Based on the logic shown in Fig. 2, the iris code is generated in stream 1 and 0. The output of the extraction feature is the quantum phase with four levels. With each filter, two bits of information are generated per pixel. The output of the quantum phase is selected for code, so that when it moves from one quarter of a circle to another, the single bit "1" changes. This is the minimum number of bits that are different, if the two intricate patterns are expressed, they become less inconsistent and thus more precise identification is provided.

Fifth step: The iris is the matching step. For this purpose, the Hamming distance is used as a criterion for identification. The Hamming distance algorithm uses only the major bits in calculating the Hamming distance between the two iris codes. Hamming distance provides a comparison of how many bits between two bit patterns are not the same. Using the Hamming distance of two bit patterns, one can decide if two patterns are produced from different irises or from the same iris. Comparing bit patterns X and Y, Hamming distance, HD, is defined as the sum of incompatible bits, that is, the sum of OR is exclusive between X and Y on N, the number of bits in the bit pattern.

$$HD = \frac{1}{N}\sum_{j=1}^{N} X_j(XOR)Y_j \quad (28)$$

Since the iris space contains high-freedom features, each iris space generates a bit pattern that is independent of the bit pattern generated by the other iris, on the other hand, two iris code generated from the same iris, which has a high correlation If both bit patterns are completely independent, so that iris patterns are

generated from the same iris, the hamming distance between the two bit patterns should be equal to 0.5. Therefore, between the two patterns, half of the bits are compatible and half of the bits are incompatible. If two patterns result from the same iris, the Hamming distance is close to 0.0, so they have a high correlation.

CONCLUSION

In general, iris detection based on a person's identification system consists of five stages: 1- segmentation, 2- normalization, 3- attribute extraction, 4- production, and 5- code matching. In the proposed method in order to extract the characteristic of iris images, the transform ripplet method was used which is one of the methods in the transform domain. In this method, Edge detector and Huff transformations are used to improve the speed and precision of the segmentation process. In the feature extraction step, in order to accurately identify individuals, most of the discriminatory information contained in the iris pattern should be extracted. The important iris features should be encrypted, so that the comparison between the patterns can be done. Most iris identification systems use iris image separator decomposition to create a biometric pattern. A pattern generated in the property encryption process also requires a matching matching criterion, which provides a similar measure between the two iris patterns. This criterion should provide a range of values at the time of comparing the patterns produced from the same eye, which is known as an intra-class comparison, and provides another range of values at the time of comparing the patterns created by different iris, which is called the comparison between a known class Gets The two should provide separate and distinct values, such that the decision can be made with certainty whether both patterns are identical in iris or from two different irises. Extracting the property is accomplished by complexizing the normalized iris pattern with one-dimensional Gabor logarithmic wavelets. A normalized two-dimensional pattern is broken up in a number of one-dimensional signals, and then these one-dimensional signals are calculated with the logarithmic Gabor wavelets using FFT and inverse FFT. Feature extraction is done at this stage using the transform ripplet in the transform domain. In the process of producing iris code, the attribute is extracted using the transform ripplet, FFT and IFFT, obtain the input for the phase quantization process in order to generate a pattern with binary values 0 and 1. This result is known as an iris code. When an iris property is extracted, the output is obtained for code generation, here a method called quantification of the phase is used to generate iris code.

REFERENCES

D.L. Donoho, M. Vetterli, R.A. Devore, I. Daubechies, Data compression and harmonic analysis, IEEE Transactions on Information Theory 44 (6) (1998) 2435–2476.

Daubechies, Ten Lectures on Wavelets, SIAM, Philadephia, PA, 1992.

S. Mallat, A Wavelet Tour of Signal Processing, second ed., Academic Press, New York, 1999.

E.J. Candes, D.L. Donoho, Ridgelets: a key to higher-dimensional intermittency?, Philosophical Transactions: Mathematical, Physical and Engineering Sciences 357 (1760) (1999) 2495–2509.

M. Do, M. Vetterli, The finite Ridgelet transform for image representation, IEEE Transactions on Image Processing 12 (1) (2003) 16–28.

S.R. Deans, The Radon Transform and Some of Its Applications, Wiley, New York, 1983.

J.L. Starck, E.J. Candes, D.L. Donoho, The curvelet transform for image denoising, IEEE Transactions on Image Processing 11 (2002) 670–684.

D.L. Donoho, M.R. Duncan, Digital curvelet transform: strategy, implementation and experiments, in: Proc. of the Aerosense 2000, Wavelet Applications VII. SPIE, vol. 4056, 2000, pp. 12–29.

E. Candes, D. Donoho, Continuous curvelet transform: I. Resolution of the wavefront set, Applied and Computational Harmonic Analysis 19 (2) (2005) 162–197.

E. Candes, D. Donoho, Continuous curvelet transform: II. Discretization and frames, Applied and Computational Harmonic Analysis 19 (2005) 198–222.

L. Hormander, The Analysis of Linear Partial Differential Operators, Springer, Berlin, 2003.

E.J. Candes, D.L. Donoho, New tight frames of curvelets and optimal representations of objects with piecewise c2 singularities, Communications on Pure and Applied Mathematics 57 (2) (2003) 219–266.

M.N. Do, M. Vetterli, The contourlet transform: an efficient directional multiresolution image representation, IEEE Transactions on Image Processing 14 (12) (2005) 2091–2106.

M.N. Do, M. Vetterli, Contourlets, in: G.V. Welland (Ed.), Beyond wavelets, Academic Press, New York, 2003.

E. Le Pennec, S. Mallat, Sparse geometric image representations with bandelets, IEEE Transactions on Image Processing 14 (4) (2005) 423–438.

D.L.D.E.J. Cands, L. Demanet, L. Ying, Fast discrete curvelet transforms, Multiscale Modeling and Simulation 5 (2005) 861–899.

Jun Xu, Lei Yang, Dapeng Wu, “Ripplet: A new transform for image processing”, Journal of Vision Communication Image Representation, 21 (2010), 627–639.